A novel locus associated with decreased susceptibility of *Plasmodium falciparum* to lumefantrine and dihydroartemisinin has emerged and spread in Uganda

Karamoko Niaré[1,2,†], Bersabeh Tafesse[3], Mayland Treat[3], Jacob M. Sadler[4], Martin Okitwi[5], Stephen Orena[5], Victor Asua[5,6], Oriana Kreutzfeld[3], Jenny Legac[3], Samuel L. Nsobya[5], Adoke Yeka[5], Philip J. Rosenthal[3], Jonathan J. Juliano[4,7,8], Jeffrey A Bailey[1,2,*], Melissa D. Conrad[3,*,†]

[1]Department of Pathology and Laboratory Medicine, Brown University, Providence, RI, USA.
[2] Center for Computational Molecular Biology, Brown University, Providence, RI, USA.
[3]Department of Medicine, University of California, San Francisco, San Francisco, California, United States of America.
[4]Institute for Global Health and Infectious Diseases, University of North Carolina, Chapel Hill, NC, USA.
[5]Infectious Diseases Research Collaboration, Kampala, Uganda.
[6]Institute for Tropical Medicine, University of Tubingen, Tubingen, Germany.
[7]Division of Infectious Diseases, School of Medicine, University of North Carolina, Chapel Hill, NC, 27599, USA.
[8]Department of Epidemiology, Gillings School of Global Public Health, University of North Carolina, Chapel Hill, NC, 27599, USA

*equal senior author contribution

†corresponding authors
Karamoko Niare, PhD
Department of Pathology and Laboratory Medicine, Brown University, Providence, RI, USA
Melissa D. Conrad, PhD
Department of Medicine, University of California, San Francisco, San Francisco, California, United States of America; melissa.conrad@ucsf.edu

ABSTRACT

Malaria control in Uganda is threatened by the emergence of artemisinin partial resistance (ART-R) and decreasing lumefantrine susceptibility. To identify loci contributing to decreased drug susceptibility, we assessed signatures of selection in Ugandan whole genome *Plasmodium falciparum* sequences. Extended shared haplotypes were seen for the ART-R associated Kelch13 (K13) C469Y and A675V mutations, but the strongest signal of recent selection was centered on a segment of chromosome 7 encoding the *phosphoinositide-binding protein* gene (*px1*, PF3D7_0720700). A haplotype, represented by three PX1 SNPs (L1222P, M1701I and D1705N) and two indels (designated PIN), was first seen in 2008 and rapidly increased, reaching prevalence >50% in northern Uganda by 2016 and eastern Uganda by 2023. PIN-carrying parasites showed significantly decreased *ex vivo* susceptibilities, measured as IC_{50}s, to lumefantrine, mefloquine and dihydroartemisinin, either with or without coincident K13 mutations. Thus, PX1 polymorphisms may impact on the susceptibilities of African malaria parasites to key drugs.

Main

Artemisinin-based combination therapies (ACTs) are the primary drugs used to treat uncomplicated *Plasmodium falciparum* malaria [1], making them a cornerstone of malaria control [2–4]. Unfortunately, the efficacy of ACTs is under threat due to the emergence of artemisinin partial resistance (ART-R), defined clinically as delayed parasite clearance following treatment with an artemisinin or *in vitro* as increased parasite survival after artemisinin exposure in the ring survival assay. This resistance is associated with treatment failures in parts of Southeast Asia [5–8] .

ART-R first emerged in Southeast Asia and appears to be primarily mediated through a number of different mutations in Kelch13 (K13), resulting in decreased parasite uptake of hemoglobin and reduced artemisinin activation [9–13]. Recently, the emergence and rapid spread of K13 mutations validated to mediate ART-R have been reported in Rwanda, Uganda, and the Horn of Africa [14–20].

The most widely used ACT in Africa is artemether-lumefantrine (AL), which was rolled out as the first-line antimalarial drug for uncomplicated malaria in Uganda in 2006. The mechanism of action of lumefantrine[2,3] is unknown. Although clinical resistance has not been identified, the *ex vivo* susceptibility of *P. falciparum* to lumefantrine in Uganda has decreased in recent years [21,22]. Decreased susceptibility to lumefantrine has been associated with polymorphisms in *P. falciparum* multidrug resistance protein 1 (MDR1) N86, 184F, 500N, 1042N and D1246, as well as chloroquine resistance transporter (CRT) K76, but high-level resistance has not clearly been identified [22–28].

Uganda is an epicenter for emerging ART-R. Five validated or candidate K13 mutations have been detected at concerning prevalences, A675V and C469Y being the most common, specifically in northern and eastern Uganda. These two mutations were first reported in northern Uganda in 2016, and have now spread across much of the country [14]. In addition, parasitological surveillance has demonstrated decreasing susceptibility to lumefantrine, first in northern Uganda, and more recently in eastern Uganda [22,25,29]. Decreased susceptibility to lumefantrine is supported by near fixation of wild-type MDR1 N86 and CRT K76 alleles, although these genotypes are associated with only small decreases in susceptibility. The clinical consequences of ART-R and decreased lumefantrine susceptibility in Uganda remain uncertain. Recent therapeutic

efficacy studies have shown corrected treatment efficacies for AL <90% at some sites [30,31], but decreased AL efficacy was not seen at the site with the highest prevalence of ART-R K13 mutations[31], and interpretation of results is confounded by the difficulty of distinguishing recrudescence and new infections after therapy in high transmission sites.

Studies of K13 flanking microsatellite haplotypes have identified independent emergences of Ugandan ART-R parasites [14], but few ART-R African isolates have undergone whole genome sequencing (WGS). To better define the genetic features of ART-R and decreasing lumefantrine susceptibility in Ugandan *P. falciparum* parasites, we performed WGS on representative isolates to characterize signals of directional selection [17,20,32].

Results

Whole genome sequencing of Ugandan isolates

Selective whole genome amplification and whole genome sequencing (WGS) was performed on 190 Ugandan *P. falciparum* samples collected from patients with uncomplicated malaria as part of ongoing molecular and parasitological surveillance [14,22,33]. Samples were selected to include include temporally matched parasites having (i) the common Ugandan K13 C469Y and A675V mutations; (ii) relatively low lumefantrine and DHA ex vivo susceptibility; or (iii) wild-type K13 sequences or relatively high lumefantrine and/or DHA *ex vivo* susceptibility. A total of 158 (82%) of the samples were successfully sequenced to a mean coverage of ≥50-fold using two Illumina Novaseq runs. After variant calling with the optimized GATK4 pipeline [34], recalibration and filtering, 55,100 high-quality SNPs with minor allele frequencies (MAF) ≥2% [35] were

obtained for downstream analysis; 118/158 infections were estimated to be mono-genomic.

Evidence of positive selection around the K13 C469Y and A675V mutations

To better understand the evolutionary history of the K13 C469Y and A675V mutations, the predominant K13 mutations in northern and eastern Uganda, we compared the extended haplotype homozygosity (EHH) of each mutation to that of the wild-type allele for monogenomic samples and for dominant strains in polygenomic infections (n=158). The K13 C469Y and A675V mutations each had a significant EHH signal, indicative of a sweep due to positive selection (**Extended Data Fig. 1A**). To determine the number of unique haplotypes associated with each mutation, we visualized and clustered the flanking variation around the *k13* gene using mono-genomic C469Y (n=15) and A675V (n=11) samples. We identified a single haplotype for C469Y as well as one major and two minor haplotypes for A675V (**Extended Data Fig. 1B**). With principal component analysis using the entire genome, samples did not cluster by K13 mutation, which suggests that significant outcrossing has occurred and that the mutation has not expanded through clonal lineages (**Supplementary Fig. 1**).

The *px1* gene shows strong signals of recent positive selection

To identify genomic variations potentially responding to AL pressure, we performed genome-wide scans of two complementary measures of positive selection: i) the IsoRelate's statistic (iR), a measurement of selection signals based on allele-level pairwise fractions of identity-by-descent (IBD), and ii) the integrated haplotype homozygosity score (iHS). The iR analysis detected 7 significant peaks: one each on

chromosomes 5, 8, 12, and 13 (the *k13* region), and 3 on chromosome 7 (**Fig**. **1A**). Analyses of samples stratified by geographical origin (north, n=116; east, n=42) (**Extended Data Fig. 2**) or by K13 genotype (675V mutant, n=31; 469Y, mutant n=35 and WT, n=92) (**Extended Data Fig. 3**) showed variation in the consistency of these signals by region and by genetic background. The iHS analysis identified many of the same regions as iR, including peaks on chromosomes 7, 8, and 12 (**Fig. 2B**, **Extended Data Fig. 4**). Additional peaks not detected by iR were seen on chromosomes 1 and 10. To focus on mutations potentially driving recent directional selection, we excluded SNPs that were: i) already common (MAF≥5%) in global *P. falciparum* samples based on the MalariaGEN Pf6 dataset or ii) under balancing selection (Tajima's D>1). With the 15,137 SNPs remaining after filtering, iHS analysis detected 11 non-synonymous mutations with significant selection signals ($P<10^{-5}$, false discovery rate (FDR)) (**Figure 1B**).

Overall, the strongest iR signal of selection (**Fig. 1A, Fig. 2A**) involving previously unidentified, rapidly increasing mutations (**Figure 2B**) was found on chromosome 7 between positions 728081 and 988719 and contained 69 genes (**Supplementary Table S1**). This candidate sweep was detected consistently in both geographical regions (although the signal was stronger in the north) (**Extended Data Fig. 2**) and in A675V, C469Y and wild-type K13 genetic backgrounds (**Extended Data Fig. 3**). Notably, of the 11 filtered SNPs with significant iHS *P* values, five fell within this chromosome 7 region (**Fig. 2B**). The maximal iHS signal co-located with the *px1* gene (PF3D7_0720700) [36]. Among all non-synonymous SNPs identified across the candidate sweep, PX1 L1222P and D1705N had the highest pairwise IBD fraction (0.03) and largest delta change in allele frequency from 2017 to 2022 (14.5% and 14.2%, respectively) (**Fig. 2C**). The iHS

signal for PX1 D1705N ($P = 1.3\ 10^{-5}$, FDR) was the highest in this genomic region and was among the strongest across the entire genome. Genes immediately proximal and distal to the peak signal in *px1* lacked significant candidate SNPs based on iHS, apart from PF3D7_0716700 and PF3D7_0721000, genes with unknown functions carrying one (R705I) and two (N2024S and E2044K) SNPs with significant iHS scores (**Fig. 2B**) and EHH plots (**Fig. 2C**), respectively [37–39]; these SNPs had lower delta changes in allele frequency (**Fig. 2B**, 2.5% for R705I, 5.5% for N2024S and 7.6% for E2044K). To further assess the five SNPs detected in the candidate sweep, we generated recombination maps of this region using all mono-genomic samples from our study (n=118) and 96 mono-genomic controls from the Tanga region in Tanzania available from MalariaGEN Pf6. Based on Tanzanian controls, all three genes were in high chromosomal crossover regions (recombination rate ρ>10) (**Extended Data Fig. 5**). Interestingly, among the Ugandan samples, the *px1* gene did not show signs of undergoing recombination, with ρ 0.78–1.97, the lowest in the candidate selection sweep. The other genes in the sweep had high recombination rates, with ρ as high as 38.8 for PF3D7_0716700 and 21.6 for PF3D7_0721000 (**Extended Data Fig. 5**).

Considering regions identified by iR, the chromosome 12 peak corresponded to the *cell-traversal protein for ookinetes and sporozoites* (*celtos*, PF3D7_1216600) gene, a major vaccine candidate [40]. The two non-PX1 iR peaks on chromosome 7, corresponding to *erythrocyte binding antigen 175* (*eba-175,* PF3D7_0731500) and *exported protein family 1 gene (epf1, PF3D7_0713200),* were only significant in eastern Uganda (**Extended Data Fig. 2**) and were not significant when stratified by K13 mutation (**Extended Data Fig. 3**). The chromosome 5 signal was no longer significant

upon stratification by region or *k13* genotype. The chromosome 8 peak corresponded to *pfa55-14* (PF3D7_0809200), which encodes the asparagine-rich antigen that was previously reported to be under directional selection in sub-Saharan African and South-East Asia [39]. This signal was present in both regions (**Extended Data Fig. 2**), but appeared to be limited to parasites carrying the wild-type K13 alle (**Extended Data Fig. 3**). The signal on chromosome 12 was limited to eastern Uganda and neared significance only in parasites carrying the wild-type K13 allele (**Extended Data Fig. 2 & 3**). Genetic regions only identified by iHS similarly corresponded to loci previously reported to show signs of positive selection in African parasite populations, consisting mainly of genes encoding known antigens, such as exported protein family1 (EPF1) and PF3D7_0710200 [39,41–43]. Thus, genes other than *px1* with iHS and iR selection signals were less compelling as encoding new candidate mediators of drug resistance, as they had characteristics consistent with evolving antigenic variation or were not consistently significant across populations, and most of them have previously been shown to be under selection in multiple countries in whole genome analyses.

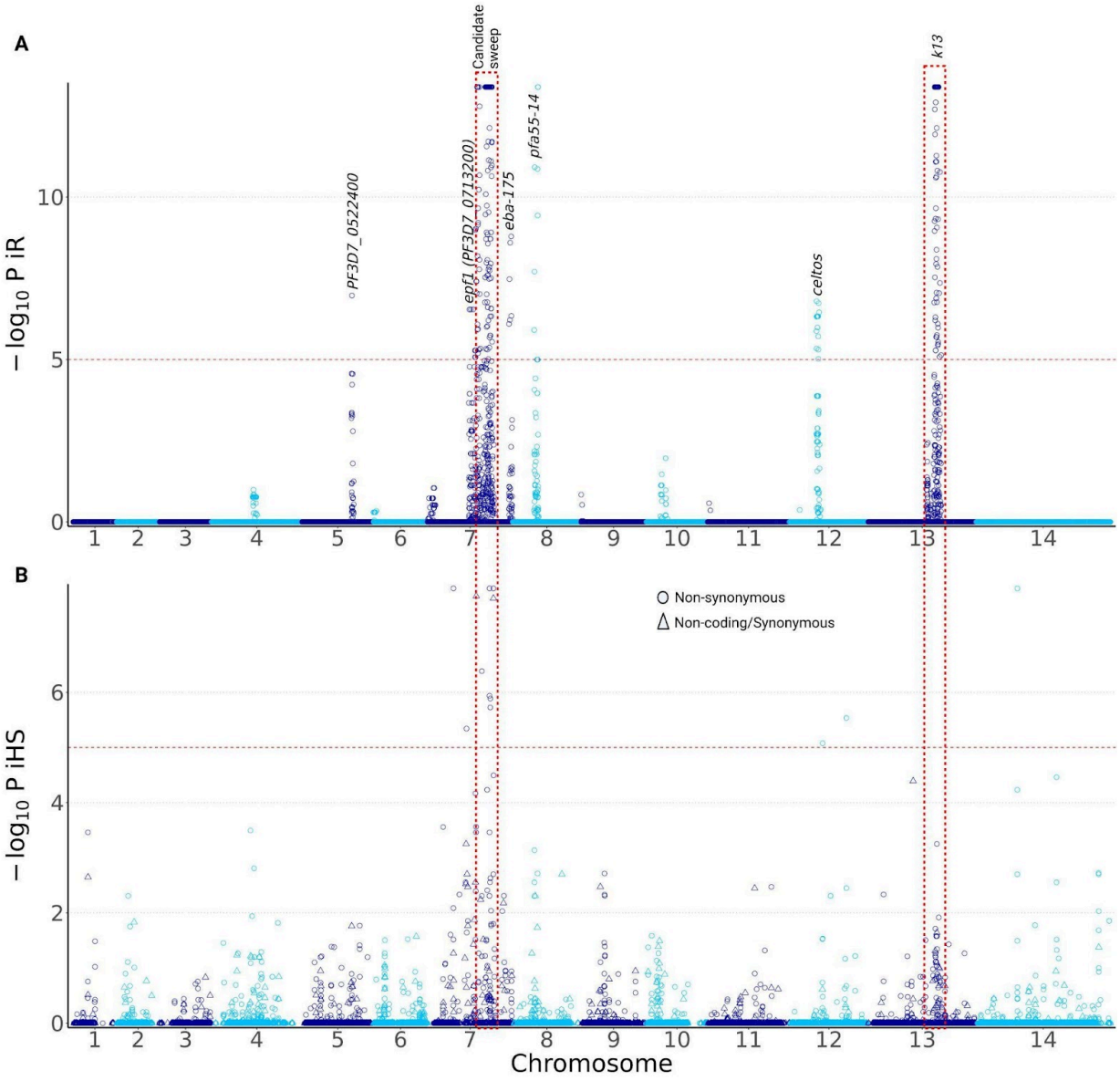

Figure 1: Selection signals across the genome. A) IsoRelate statistic based on IBD across the genome in all samples (n=158). *P* values were corrected for multiple testing using false discovery rate (FDR). This analysis included all SNPs with minor allele frequency ≥2%. **B)** Integrated haplotype homozygosity scores (iHS) across the genome identifying coding changes in monogenomic samples (n=118). SNPs with MAF<2% in our dataset or Tajima's D>1 or MAF≥5% in the global Pf6 dataset were excluded. *P* values were corrected for multiple testing using FDR. Significance thresholds of -Log_{10}(FDR-corrected *P* value) = 5 are indicated by the dotted horizontal line. The vertical dotted lines indicate regions with the strongest iR signals.

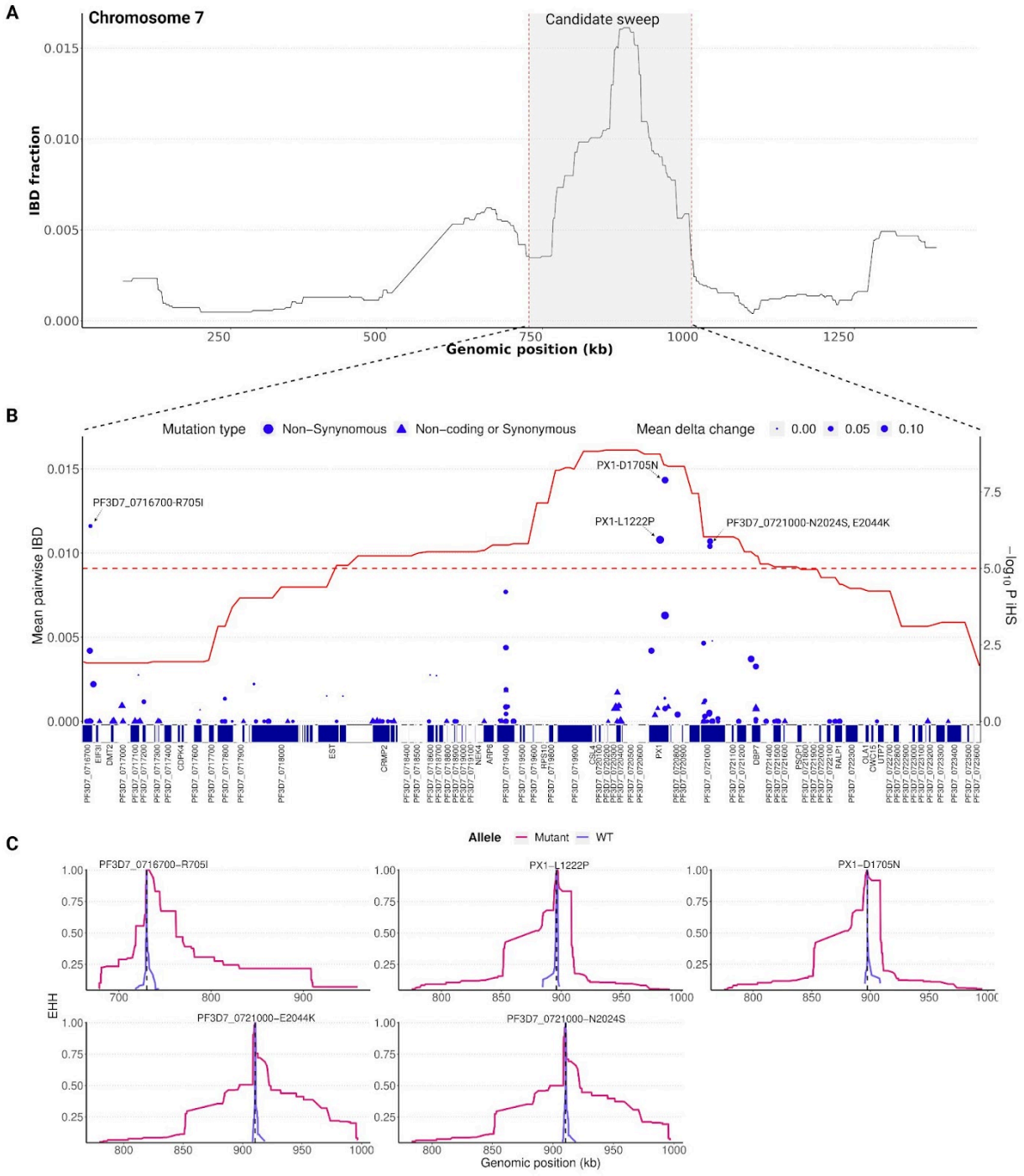

204

205 **Figure 2**: **A dominant selection signal around the *px1* gene**. **A)** Allele-level pairwise
206 IBD fractions along chromosome 7. The peak corresponding to the candidate sweep
207 based on iR and iHS is indicated. **B)** iHS measure of selection signatures and
208 allele-level pairwise IBD fractions within the candidate sweep region
209 (Pf3D7_07_v3:728081–988719). The red curve represents the pairwise IBD fraction; its
210 values are shown on the left y-axis. The significance of iHS is indicated on the right

y-axis. The delta change of allele frequency over time for each SNP is represented by the size of the iR and iHS dots. Annotation of genes and SNPs within the candidate sweep is shown in the x-axis. The top non-synonymous SNPs with significant iR and iHS and high IBD fraction within the candidate sweep are indicated. **C)** High extended haplotype homozygosity (EHH) around top SNPs (all non-synonymous) showing significant iR and iHS relative to the wild-type (WT). Only SNPs with MAF≥2% in mono-genomic samples were used for this analysis (n=118). Mutant represents the derived allele.

A haplotype block centered around the *px1* gene.

Visualization and clustering of variation in the candidate sweep region (~260kb, Pf3D7_07_v3:728081–988719) was performed using sequences from mono-genomic samples with no coverage gaps (L1222P and D1705N mutant, n=48; wild-type, n=21) and indicated that all implicated SNPs belonged to a single shared haplotype (**Supplementary Fig. 2**). Although the length of this haplotype varied by isolate, the most conserved segment across samples (Pf3D7_07_v3:873,736–918,738) coincided with the peak of IBD fractions (**Fig. 3A, Supplementary Fig. 2**) including 12 genes with *px1* at the center. We named this shared haplotype PIN for the three SNPs, L1222P, M1701I, and D1705N, with the highest frequency changes and measures of EHH. The PIN haplotype was found in 58.2% of isolates sequenced and the wild-type haplotype, LMD, in 28.5%. All other detected haplotypes (LID, LIN, PID, PMD and PMN) were represented in <10% of isolates. Two other SNPs (D384A and S1673N) were weakly associated with the PIN haplotype: the D384A mutation was present in 82.8% of PIN samples (77 out of 93) but showed a non-significant iHS score ($P > 10^{-5}$, FDR), and the S1673N mutation was present in all PIN samples and showed a non-significant iHS score ($P = 0.18$, FDR). Of note the S1673N mutation was also present in 66.7% of non-PIN haplotype samples and appeared at high frequency in the Pf6 dataset. Overall,

sampling locations and K13 mutations were not associated with clustering within the PIN genomes (**Supplementary Fig. 2**). The shared haplotype appeared to shorten over time, particularly in northern Uganda (**Supplementary Fig. 2**).

The *px1* gene contains 4 exons and measures ~9 kb, with conserved C-terminal and N-terminal regions (**Fig. 2B**). Candidate SNPs are located in exon 3, which measures 5.78 kb (nucleotides 892,083-897,457) and also encodes a repetitive region with evidence for deletions (**Supplementary Fig. 3**). Oxford Nanopore Technologies (ONT) long-read sequencing tiling the *px1* gene resolved five in-frame deletions within the coding sequence of 24 representative mono-genomic samples and controls (**Supplementary Table 3**, **Supplementary Fig. 3 and 4**). Among the deletions in the PIN haplotype, two ($del_{V1680\text{-}N1685}$ and $del_{N811\text{-}Y822}$, deletions of 18 and 36 nucleotides at positions 897,247 and 894,638, respectively) were uncommon (MAF<5%) in the Pf6 dataset and showed high EHH signal in our Uganda WGS data (**Extended Data Fig. 5**).

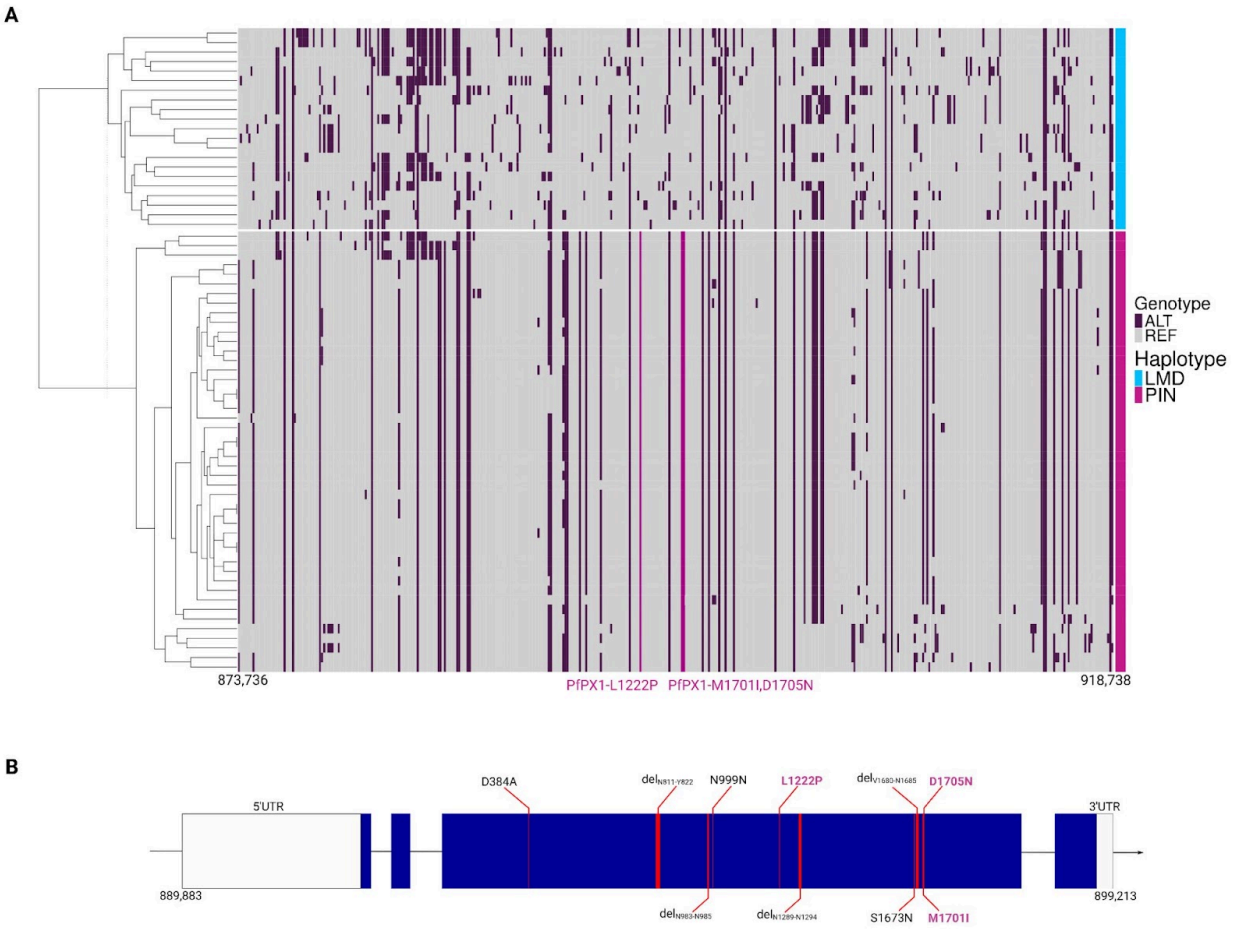

Figure 3: **Shared haplotype in the chromosome 7 region**. **A)** Haplotypes are based on SNPs called by GATK4 in mono-genomic samples at minor allele frequency ≥2%. Hierarchical clustering of haplotypes is shown on the left. The region shown corresponds to the peak of IBD fractions in chromosome 7 (Pf3D7_07_v3:873,736–918,738). Positions of key mutations (PX1 L1222P, M1701I and D1705N) in the *px1* gene are indicated by vertical pink lines. Sample genotypes, either PIN (triple mutations) or LMD (wild-type), are shown on the row (right). ALT is the alternate genotype coded as 2 and REF is the reference (3D7) genotype coded as 0 in the heatmap. **B)** Diagrammatic illustration of the *px1* haplotype solved by long read sequencing. Indels and SNPs are indicated. Key SNPs and in-frame deletions are highlighted in pink. Blue boxes represent exons. Horizontal lines represent introns. Empty boxes indicate 5' and 3' untranslated regions (UTRs). The gene is transcribed from the positive strand.

The prevalence of the PX1 PIN haplotype has been increasing rapidly in Uganda.

To better assess spatiotemporal variation in the prevalence of PX1 PIN haplotypes, we genotyped 1,598 samples collected from eastern Uganda in 2004, 2008, and 2012, and from eastern and northern Uganda from 2016–2024. Using two of the primers designed to tile the *px1* gene, a 2.6kb region (894851–897457) spanning all the key variants was amplified and ONT sequenced (**Supplementary Table 3, Supplementary Fig. 3**). A total of 1,436 samples had sequencing coverage ≥25X and underwent haplotype calling. In 2004, before ACTs were recommended for treatment of malaria in Uganda, the most common haplotypes seen were LMD (76.9%) and LID (12.1%); the PIN and PMN haplotypes were not found (**Fig. 4)**. The PIN haplotype was first seen in 2008, with significantly increasing prevalence over time in both regions, reaching 55% in eastern (*P=0.009,* Mann-Kendall Test*)* and 84% in northern (*P=0.009*, Mann-Kendall Test*)* Uganda in 2024 **(Fig. 4)**. The same trend was observed after analyzing the prevalence over time by sampling site using a Bayesian model **(Supplementary Fig. 4)**.

We evaluated the co-occurrence of K13 and putative ACT partner drug resistance mutations as well as PIN haplotypes in samples from northern Uganda, where K13 mutations first emerged and were more prevalent than in other regions[14]. Compared to wild-type K13, the C469Y and A675V mutations were consistently more prevalent in parasites carrying the PIN haplotype over time, although statistical assessment was limited by small sizes upon stratification (**Supplementary Fig. 5**). The proportions of MDR1, CRT, dihydrofolate reductase (DHFR) and dihydropteroate synthase gene (DPHS) mutations associated with resistance to other antimalarials were similar in PIN and LMD parasites, suggesting no co-occurrence of these markers with the PIN haplotype (**Supplementary Fig. 6**) .

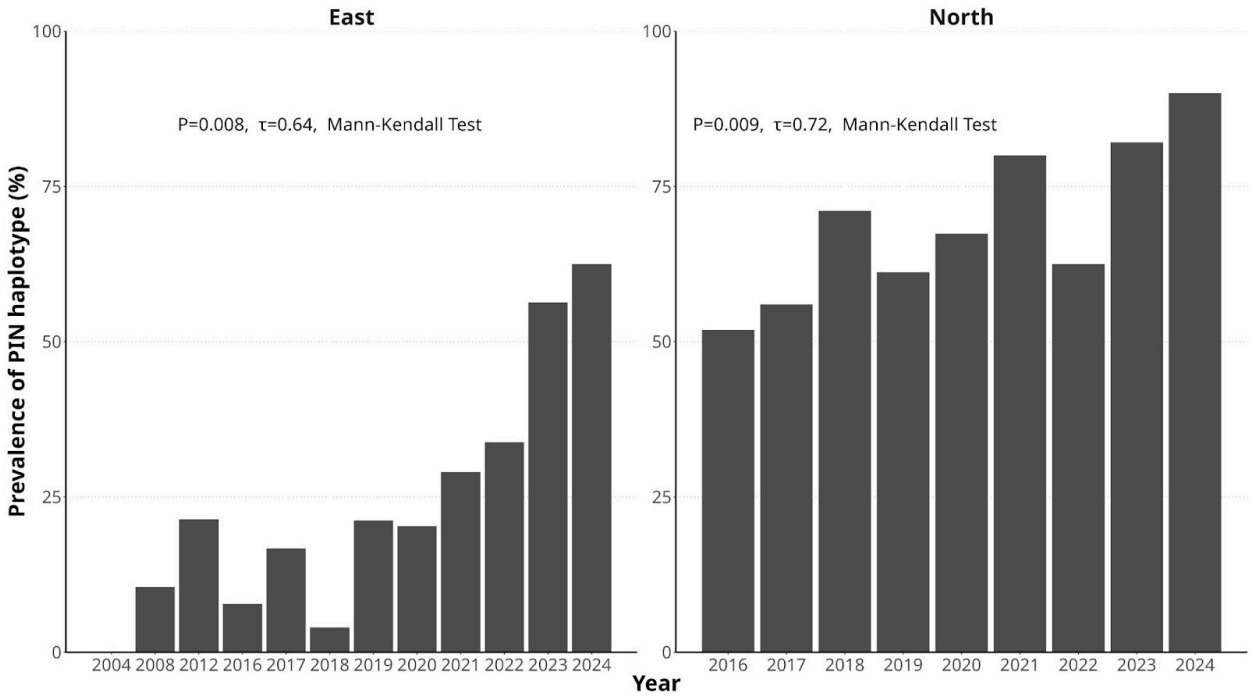

Figure 4: **Prevalence of PX1 PIN haplotypes over time in eastern and northern Uganda**. Kendall's correlation coefficient (τ) and the significance of the trend of PIN haplotype prevalence (Mann-Kendall Test) are indicated. Sample size for each year is shown on top of the bar. Sample sizes for the east were : n=88 (2004), n=2008 (n=86), n=49 (2016), n=54 (2017), n=50 (2018), n=66 (2019), n=69 (2020), n=93 (2021), n=71 (2022), n=71 (2023) and n=48 (2024). Sample sizes for the north were: n=52 (2016), n=50 (2017), n=45 (2018), n=49 (2019), n=95 (2020), n=55 (2021), n=80 (2022), n=39 (2023) and n=50 (2024).

The PX1 PIN haplotype was associated with reduced *ex vivo* susceptibility to DHA and lumefantrine

We evaluated associations between the PX1 haplotypes and *ex vivo* drug susceptibility [22], considering samples with ≥25X sequencing depth in which the called allele represented ≥90% of reads to reduce ambiguity introduced by mixed genotype infections (n=465). Overall, the PIN haplotype was associated with decreased DHA, lumefantrine and mefloquine susceptibilities (increased IC_{50}s) compared to the WT

(LMD) haplotype (*P<0.001* for all comparisons, Wilcoxon Test; **Supplementary Fig. 7**). When considering samples with wild-type K13, the PIN haplotype was associated with decreased susceptibility compared to the LMD haplotype for lumefantrine (median IC_{50} [interquartile range]: 14.3 nM [9.8–24.0], n=110 vs. 6.2 nM [4.4–10.5 nM], n=240), mefloquine (17.1 nM [10.4–26.7], n=109 vs. 11.0 nM [7.7–16.0], n=236), and DHA IC_{50} (3.7 nM [2.4–5.5], n=110 vs. 1.8 nM; [1.2–2.6], n=240) (**Fig. 5**). Similar trends were seen with samples carrying the K13 C469Y mutation, although the small number of isolates with the PIN haplotype and C469Y (n=25) limited assessment of statistical significance (**Supplementary Fig. 8)**. These trends were seen when stratifying samples based on year or geographical origin (**Supplementary Fig. 9A and 9B**). Notably, no differences in *ex vivo* RSA survival between haplotypes were detected, consistent with our recent observation that *ex vivo* RSA results from 2019-2024 did not correlate with other markers of drug susceptibility in Uganda [22].

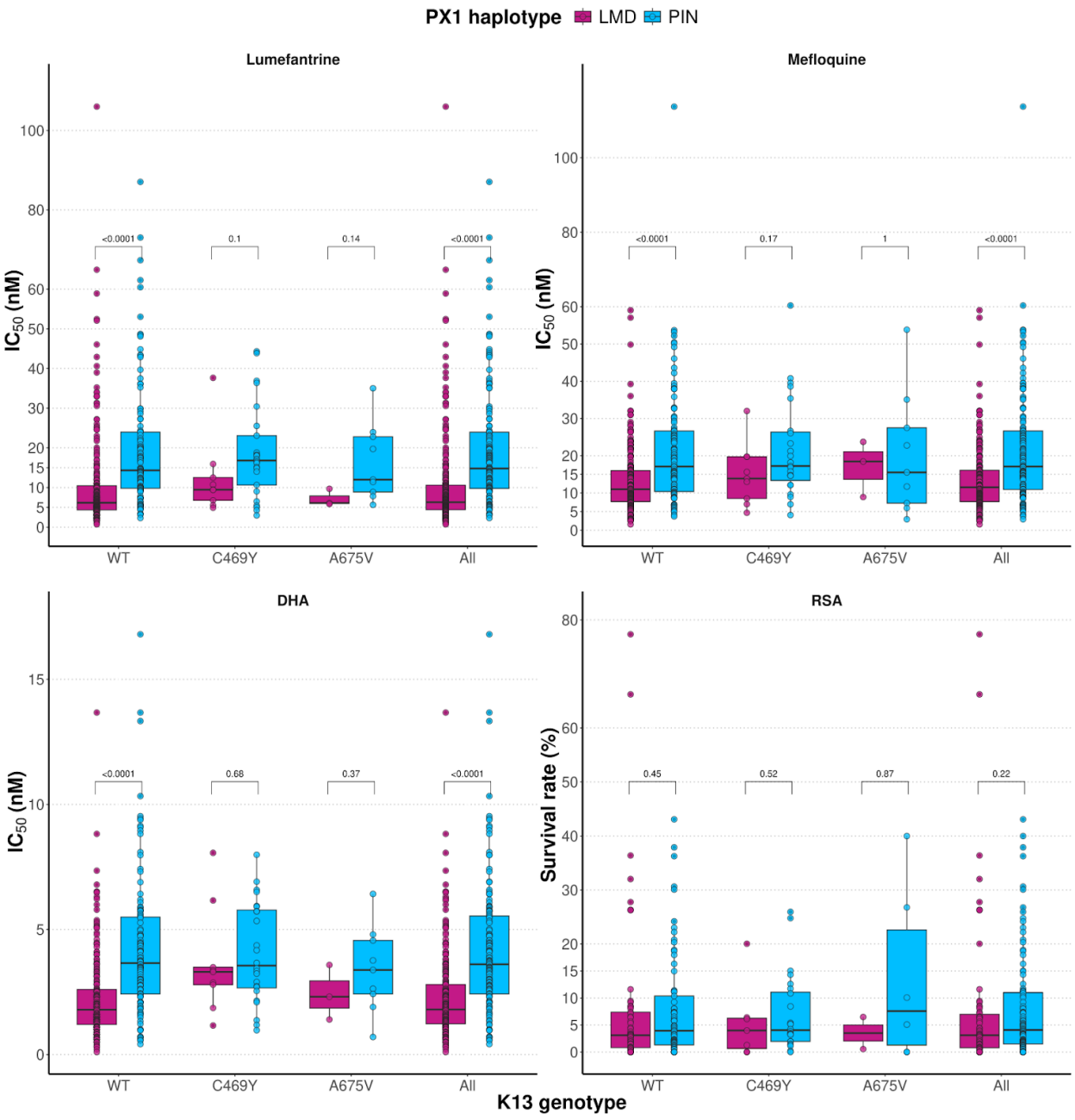

Figure 5. E*x vivo* drug susceptibility of PX1 haplotypes. Shown are *ex vivo* half-maximal inhibitory concentrations (IC_{50}s) for the indicated drugs and DHA ring-stage survival assay results for PX1 PIN and LMD haplotypes. Analysis was stratified by Kelch13 (K13) mutation status. Only samples with read depth ≥25X were included (n=465). Only major alleles supported by at least 90% of reads were selected. *P*-value (Wilcoxon Test) is shown for each comparison.

The PX1 PIN haplotype was rare in assessments of global parasite populations in the Pf6 dataset

The Pf6 WGS dataset, which includes samples collected between 2001 and 2015 (6,388 samples), [44] was mined to examine the global distribution of different PX1 alleles [34]. Overall, PX1 allele frequencies varied geographically; the PIN haplotype was not found outside of Africa (**Supplementary Fig. 10, Supplementary Fig. 11**). In Africa, we detected the PIN haplotype in only 5/3570 samples, including 3 from The Democratic Republic of Congo (DRC, 2 in 2012 and 1 in 2014, n=364) and 2 from Kenya (both in 2014, n=110), in all but one as a mixed genotype. The PMN haplotype was found in one polygenomic sample from Kenya in 2014. The LID haplotype was seen at high prevalence in Africa, South-Asia, and South America (**Supplementary Fig. 11**). The LIN haplotype was at a maximum prevalence of 9.3% (34/364) in DRC.

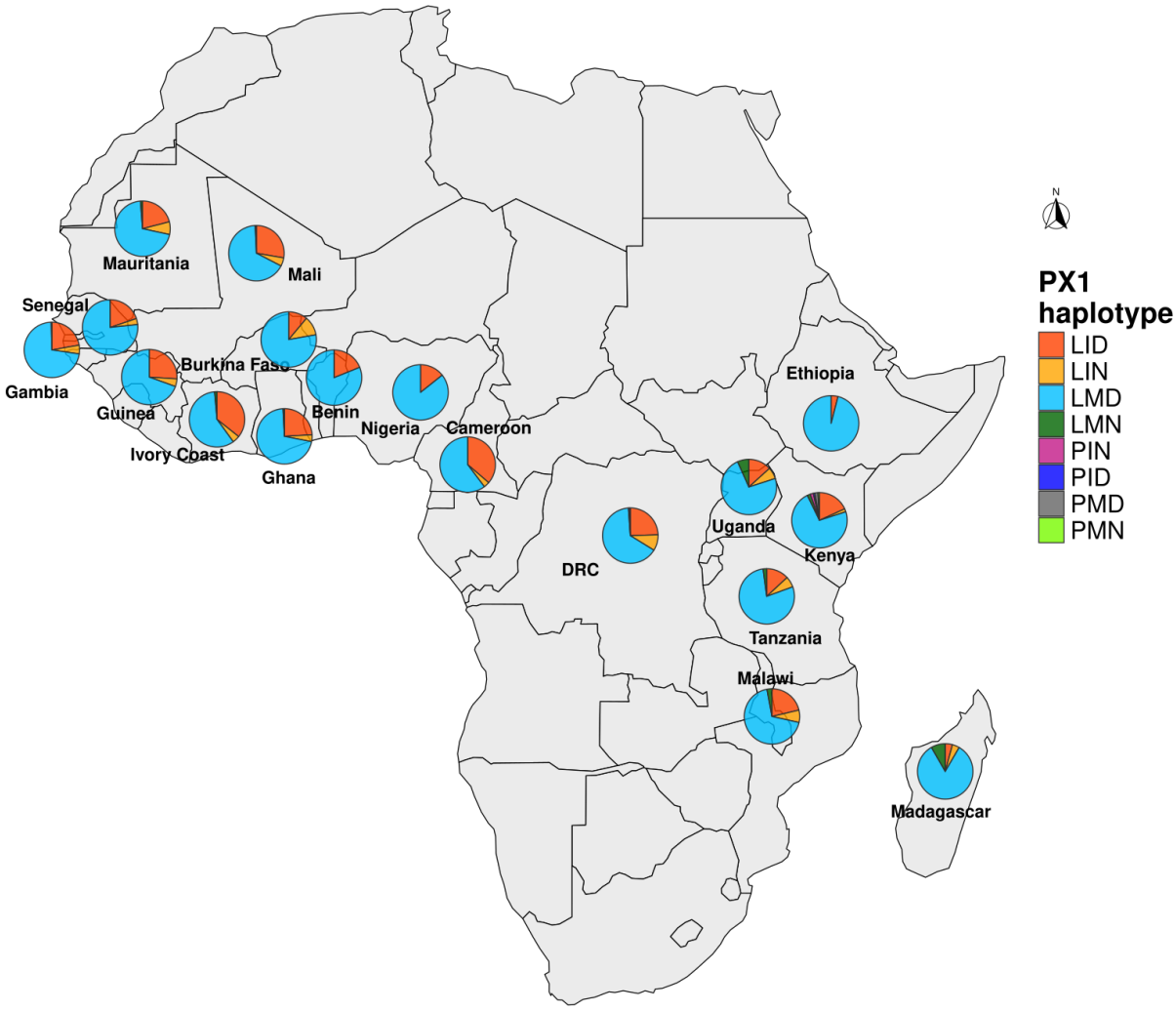

341

342 **Figure 6. Distribution of PX1 haplotypes in Africa in 2011–2015.** The presence of 3
343 key amino acids that define the PIN haplotype, representing true haplotypes or
344 co-occurrence of alleles within isolates is shown for 6,388 MalariaGEN Pf6 dataset
345 samples from 18 countries. DRC: Democratic Republic of Congo.

346

347

348

Discussion

The decreased lumefantrine susceptibility and emergence of ART-R K13 mutations reported in Uganda [14,22,25,29,45–47] raise a major concern for malaria control in Africa, prompting a comprehensive search for genomic regions of directional selection that might underlie these changes. We leveraged WGS of Ugandan *P. falciparum* isolates with varied K13 sequences and *ex vivo* drug susceptibilities to identify a novel locus associated with decreased susceptibility to DHA and lumefantrine, the most widely used antimalarial drugs in Africa. Based on iR and iHS analyses, the strongest signal of recent selection was on chromosome 7, centered on the *px1* gene. The PX1 PIN haplotype carrying L1222P, M1701I, D1705N mutations and two deletions showed the strongest signal of selection, with long flanking haplotypes. This haplotype was not detected in samples collected in 2004, before rollout of AL in Uganda, but increased in prevalence thereafter. Thus, the PX1 PIN haplotype appears to have emerged in Uganda before K13 mutations. K13 mutations may have emerged on this background, as a high proportion of parasites collected from northern Uganda with C469Y or A675V mutations also contained the PIN variant. Importantly, isolates with the PIN haplotype had significantly decreased susceptibilities to lumefantrine and DHA compared to parasites with the wild-type PX1 haplotype.

Our evidence suggests that *px1* has been the target of strong directional selection in Ugandan malaria parasites, leading to a steady increase in frequency of the PIN haplotype. The candidate sweep signal encompassed a large region (~260kb) containing 69 genes, among which a core haplotype (Pf3D7_07_v3:873,736–918,738)

of 12 genes, including *px1,* showed limited recombination. Our identification of *px1* as the selection target was based on an array of evidence. First, *px1* was in the center of the iR peak, a *P. falciparum*-optimized measure of selection [48]. Second, this peak had the highest IBD fractions across the genome. Third, the PX1 D1705N mutation had the strongest iHS and EHH signals among all SNPs located within the candidate sweep region. Fourth, L1222P and D1705N mutation frequencies had the highest delta changes over time. Fifth, there was an abundance of synonymous and non-coding SNPs surrounding the *px1* gene, a strong indicator of genetic hitchhiking resulting from rapid selection. Sixth, *px1* had the lowest recombination rates among all the genes located within this candidate sweep.

The identification of emergence of the PIN haplotype in northern Uganda has important implications for our understanding of the spread of ART-R and decreased lumefantrine susceptibility in northern Uganda. Our findings suggest that PIN emerged in northern Uganda prior to the emergence of the K13 mutations clearly linked to ART-R, with identification of the haplotype in samples collected in 2008. The K13 469Y and 675V mutations were first seen in samples collected much later, in 2016. The subsequent enrichment of C469Y and A675V in PIN-carrying parasites suggests that ART-R emergence may have been facilitated by the presence of the PIN haplotype. The PIN haplotype is now present in the vast majority of parasites in northern Uganda and appears to be rising quickly in eastern Uganda. In addition, emergence of the PIN haplotype was temporally and geographically associated with decreasing susceptibility to lumefantrine, which was first seen in northern, and later in eastern Uganda [21,22,25,29].

Overall, these findings suggest that heavy exposure to AL, beginning in about 2006, led to selection of the PX1 PIN haplotype and then the K13 mutations that mediate ART-R.

Although the PIN haplotype was often seen in K13 mutant parasites, decreased lumefantrine susceptibility was linked to this haplotype independent of K13 mutations associated with ART-R or of MDR1 mutations linked to decreased lumefantrine susceptibility. Interestingly, the rising prevalence of the PIN haplotype is coincident with decreasing lumefantrine susceptibility, first in northern, and later in eastern Uganda, at a time when the MDR1 N86 wild-type sequence had become fixed [21,22,25,29,45–47]. In addition to association with lumefantrine susceptibility, the PIN haplotype was associated with decreased DHA susceptibility even in the absence of K13 mutations. Thus, remarkably, PX1 mutations are associated with, and may mediate decreased susceptibility to both components of AL.

Limited experimental evidence supports a role for PX1 polymorphisms in ART-R. Experimental inactivation of the *px1* gene, which encodes a putative phosphoinositide-binding protein, conferred a growth defect, decreased transport of hemoglobin to the parasite food vacuole, and artemisinin resistance [36]. These data are consistent with PX1 playing a role similar to that of K13, in facilitating efficient transport of hemoglobin to the food vacuole. Prior data suggests that PX1 binds phosphatidylinositol-3-phosphate and localizes to membranes of hemoglobin transport vesicles and the food vacuole [36]. Thus, in a manner similar to K13 mutations that mediate ART-R, PX1 mutations may lead to decreased hemoglobin transport, and thereby decreased artemisinin activation in the food vacuole [12,36]. Our sequencing did not identify mutations in the proposed phosphoinositide-binding domain of PX1, but one

of the deletions associated with the PIN haplotype ($del_{N811\text{-}Y822}$) was located between two transmembrane domains, such that it might interfere with protein function [36] (https://plasmodb.org/plasmo/app/record/gene/PF3D7_0720700#category:protein-properties). In addition, truncation of the region of the *px1* gene containing PIN-associated variations was unsuccessful [36]. These results suggest that PIN polymorphisms alter PX1 function, leading to ART-R either in concert with or independent of K13 mutations. However, the association between PX1 mutations and decreased lumefantrine susceptibility is unexplained. Indeed, this is also the case for the association between K13 mutations and decreased lumefantrine susceptibility [21,22]. Mutations in K13 and PX1 are clearly associated with decreased lumefantrine susceptibility, but the biological basis of this association is unknown.

Materials and methods

Study design and sample collection.

For WGS activities, we leveraged clinical samples collected as part of ongoing health facility-based molecular [14,33,49] and parasitological [21,22] surveillance activities (**Supplementary Methods**). Briefly, molecular surveillance samples were collected from patients >6 months of age diagnosed with malaria by rapid diagnostic test or microscopy at up to 16 health facilities (**Fig.S13**) across the country between 2016 and 2024. Following consenting, dried blood spots (DBS) were collected by finger prick. For parasitological surveillance, patients >6 months of age diagnosed with high parasitemia malaria by microscopy at health facilities (**Fig.S13**) near parasitology laboratories in

Tororo, Tororo District in eastern Uganda and Kalongo, Agago District in northern Uganda between 2016 and 2024 were consented and up to 5mL of blood was collected into heparin tubes by venipuncture. From these samples, we selected low complexity of infection samples based on K13 mutation, low lumefantrine and/or DHA susceptibility, or high RSA survival. Each of these samples was then matched by collection year and site with a low complexity of infection sample encoding a WT K13 allele or having unremarkable lumefantrine and DHA susceptibility profiles.

To estimate prevalences of PX1 genotypes over time, we performed long read ONT sequencing (**Supplementary Methods**) on a random subset of 50 samples that had undergone *ex vivo* drug susceptibility assessment from each site for each year of surveillance activity (50 each year from 2016-2024 for the eastern region and 50 each year from 2021 to 2024 for the northern). For each year when *ex vivo* samples were not available from the north, we sequenced a random subset of 50 molecular surveillance samples collected from the Patongo health facility. Finally, to provide an understanding of changes in *px1* diversity in the early stages of AL utilization, we evaluated 91 pre-treatment samples collected as part of a 2004 therapeutic efficacy study [50] and 92 samples collected per year in 2008 and 2012 from children (aged < 5 years) enrolled in a cohort study. Both studies were conducted in Tororo.

For these studies, consent for future use of biological samples was given for all samples and ethical approval was obtained from the Makerere University Research and Ethics Committee, the Uganda National Council for Science and Technology, and the University of California, San Francisco, Human Research Protection Program.

Library preparation, whole genome sequencing and variant calling.

Genomic DNA extracted from DBS underwent two rounds of specific whole genome amplification (sWGA) as previously described [51]. The amplified products were combined, and whole genome sequencing libraries were prepared using the Watchmaker DNA Library Kit with Fragmentation (Watchmaker Genomics Inc., Boulder, CO). The resulting libraries were pooled and sequenced using Illumina 2×150bp chemistry at the Psomagen on an Illumina X Plus© (Psomagen, Rockville, MD). After sequencing, Trimmotic was used to trim off adapters and select properly paired reads before mapping. Reads were competitively mapped onto a hybrid reference genome obtained from the concatenation of *P. falciparum* 3D7 (version 3.1) and human genome assembly (version GRCh38) using BWA-MEM. We used Samtools and GATK to select and clean reads that specifically mapped to the *P. falciparum* genome. Samples with human/parasite read ratio <10 were retained and those among these with low sequencing depth (first quartile of read depth <35X) were repooled and rebalanced for another Novaseq X plus© run. Cleaned binary alignment map (BAM) files from different sequencing runs were merged before variant calling using a *P. falciparum*-optimized GATK4 pipeline (https://github.com/Karaniare/Optimized_GATK4_pipeline/tree/main) as previously described [34]. An accurate *in silico* positive training dataset built in the pipeline was used for machine learning variant recalibration accounting for multiple mapping parameters including read depth, mapping quality and strand bias. Variants that failed this filtering were removed as well as samples and variants with genotype missingness >10 and 20%, respectively. Subtelomeric and internal hypervariable regions that are hard to map were excluded from the variant call format (VCF) file to focus the

downstream analysis on the core genome as previously defined [52]. The fraction of reads supporting the alternate allele was added in the format field to enable detection of major alleles in mixed infection samples.

Estimation of complexity of infection.

We selected high-quality SNPs with MAF ≥2% to estimate COI using THE REAL McCOIL package [53] as implemented in the MIPTools pipeline. The total number of Markov chain Monte Carlo was set to 2000 with 500 burn-in iterations.

Selection analysis.

The *rehh* R package was employed to estimate the EHH around specific makers and to scan the genome for iHS signals at the allele-level using filtered VCFs. An initial analysis was performed with all the SNPs at MAF ≥2% in mono-genomic samples. Tajima's D analysis was also performed in this SNP set to identify balancing selection signals, likely due to immune pressure. In the subsequent iHS scan, we excluded SNPs with Tajima's D>1 or that were already at MAF≥5% in the MalariaGEN Pf6 dataset in samples collected until 2015, in order to detect signals of recent directional selection. To test whether a SNP is under significant iHS selection, the P value was computed using the formula $P = -\log_{10}(2\Phi(-|iHS|))$ where $\Phi(x)$ is the normal distribution function [54]. The size of allele frequency bins used to standardize the ratio between derived and ancestral alleles was 50. The minimum absolute number of evaluated haplotypes was set at 4. Multiple testing corrections were done using FDR.

The IsoRelate iR statistics was also used to scan the genome for recent positive selection signals based on IBD [48]. A potential genotyping error of 0.001 was admitted in

principle for the IBD calculation using all the SNPs at MAF ≥2% after recalibration filtration. A minimum shared IBD segment of 50kb based on at least 20 SNPs between sample pairs was considered. The IsoRelate function *getIBDiR* was used to estimate the significance of pairwise iR statistics per SNP across the entire sample set and after stratification either by K13 mutations or sampling regions. Multiple testing corrections were also done using FDR.

To further characterize the selection sweeps detected across the genome, the SnpEff annotations were used to identify whether SNPs are non-synonymous or synonymous or from non coding regions. The delta changes of allele frequencies for these SNPs over time were also calculated. For more robust analysis of spatiotemporal change in PX1 mutations, prevalences of detected haplotypes were calculated from 2008-2024 in the east and from 2016-2024 in the north. Linear regression model was used to measure the increase of haplotype frequencies over time in each region.

Statistical analysis

Data analysis was performed using R (version 4.3.1). We used Mann-Kendall Test for the trend analysis of haplotype prevalence over time in northern and eastern Uganda. The trend by sampling site was analyzed using the Bayesian model as previously described [55]. To evaluate genotype-phenotype associations, we utilized all samples with lumefantrine, DHA or mefloquine IC_{50}s or RSA data that underwent *px1* and *k13* sequencing. Wilcoxon rank-sum test (independent sample sets, two-sided) was used to compare phenotype scores (IC_{50}s or RSA survival rates) between PX1 haplotypes (PIN and LMD) with stratifications by different variables including K13 WT, 675V and C469Y

alleles, region and year. P values < 0.05 indicated statistically significant differences. Complete-linkage hierarchical clustering method was used to cluster haplotypes flanking the *px1* gene based on the genotype matrix in mono-genomic samples.

Contributions

KN, MDC, JJJ, JAB and PJR designed and conducted the study. KN analyzed data and interpreted results. MDC, JJJ and JAB supervised the analysis and interpretation of the data. MDC obtained primary funding and led the project. JJJ and JS performed the library preparation for whole genome sequencing. KN and BF performed Nanopore sequencing. MT, OK and JL performed genotyping assays. MO, SO, VA, SN and AY performed ex vivo assays. KN wrote the primary draft of the manuscript. KN, MDC, JJJ, JAB, PJR significantly reviewed and polished the manuscript. All authors contributed to the writing of the manuscript.

Acknowledgements

This work was funded by the National Institutes of Health (NIH)/National Institute of Allergy and Infectious Diseases (NIAID) (R01AI173557 to MDC and K24AI134990 to JJJ). Sample collection and phenotyping was funded by NIAID (R01AI075045, U19AI089674, R01AI117001 and R01AI139179); the Medicines for Malaria Venture (RD/15/0001); and the Gates Foundation (INV-035751). The authors are grateful to the study participants, caregivers and research teams at the Infectious Diseases Research Collaboration (IDRC) in Uganda. The funders had no role in study design, data collection, analysis, interpretation or the decision to publish. The authors are thankful to Shreeya Garg for performing molecular assays; Patrick K. Tumwebaze, Oswald Byaruhanga,

Evans Muhanguzi, Solomon Opio, Innocent Tibagambirwa, Patrick Angutoko, Jackson Asiimwe, Yoweri Tarema and Thomas Katairo for performing ex vivo assays; and Grant Dorsey for sharing metadata for historical samples. In memory of Roland Cooper.

Ethics declarations

Competing interests

The authors declare no competing interests.

Data availability

Parasite whole-genome sequences that support the findings of this study have been deposited in the Sequence Read Archive (http://www.ncbi.nlm.nih.gov/bioproject/1298911) repository and are accessible under the accession numbers SAMN50288312 to SAMN50288469.

Reference

1. WHO. *World Malaria Report 2024*. https://www.who.int/teams/global-malaria-programme/reports/world-malaria-report-2024 (2024).
2. Shibeshi, W., Alemkere, G., Mulu, A. & Engidawork, E. Efficacy and safety of artemisinin-based combination therapies for the treatment of uncomplicated malaria in pediatrics: a systematic review and meta-analysis. *BMC Infect. Dis.* **21**, 326 (2021).
3. Makanga, M. & Krudsood, S. The clinical efficacy of artemether/lumefantrine (Coartem®). *Malar. J.* **8**, 1–12 (2009).

4. Balint, G. A. Artemisinin and its derivatives: an important new class of antimalarial agents. *Pharmacol. Ther.* **90**, 261–265 (2001).

5. Dondorp, A. M. *et al.* Artemisinin resistance in Plasmodium falciparum malaria. *N. Engl. J. Med.* **361**, 455–467 (2009).

6. Witkowski, B. *et al.* Novel phenotypic assays for the detection of artemisinin-resistant Plasmodium falciparum malaria in Cambodia: In-vitro and ex-vivo drug-response studies. *Lancet Infect. Dis.* **13**, 1043–1049 (2013).

7. Amaratunga, C. *et al.* Dihydroartemisinin-piperaquine resistance in Plasmodium falciparum malaria in Cambodia: a multisite prospective cohort study. *Lancet Infect. Dis.* **16**, 357–365 (2016).

8. Phyo, A. P. *et al.* Declining efficacy of artemisinin combination therapy against P. falciparum malaria on the Thai-Myanmar border (2003-2013): The role of parasite genetic factors. *Clin. Infect. Dis.* **63**, 784–791 (2016).

9. Mok, S. *et al.* Population transcriptomics of human malaria parasites reveals the mechanism of artemisinin resistance. *Science* **347**, 431–435 (2015).

10. Rocamora, F. *et al.* Oxidative stress and protein damage responses mediate artemisinin resistance in malaria parasites. *PLoS Pathog.* **14**, e1006930 (2018).

11. Rahman, A. *et al.* Artemisinin-resistant Plasmodium falciparum Kelch13 mutant proteins display reduced heme-binding affinity and decreased artemisinin activation. *Commun. Biol.* **7**, 1499 (2024).

12. Birnbaum, J. *et al.* A Kelch13-defined endocytosis pathway mediates artemisinin resistance in malaria parasites. *Science* **367**, 51–59 (2020).

13. Rosenthal, P. J., Asua, V. & Conrad, M. D. Emergence, transmission dynamics and

mechanisms of artemisinin partial resistance in malaria parasites in Africa. *Nat. Rev. Microbiol.* **22**, 373–384 (2024).

14. Conrad, M. D. *et al.* Evolution of Partial Resistance to Artemisinins in Malaria Parasites in Uganda. *N. Engl. J. Med.* **389**, 722–732 (2023).

15. Uwimana, A. *et al.* Emergence and clonal expansion of in vitro artemisinin-resistant Plasmodium falciparum kelch13 R561H mutant parasites in Rwanda. *Nat. Med.* **26**, 1602–1608 (2020).

16. Young, N. W. *et al.* High frequency of artemisinin partial resistance mutations in the great lake region revealed through rapid pooled deep sequencing. *bioRxiv* (2024) doi:10.1101/2024.04.29.24306442.

17. Juliano, J. J. *et al.* Country wide surveillance reveals prevalent artemisinin partial resistance mutations with evidence for multiple origins and expansion of high level sulfadoxine-pyrimethamine resistance mutations in northwest Tanzania. *medRxiv* (2023) doi:10.1101/2023.11.07.23298207.

18. Mihreteab, S. *et al.* Increasing prevalence of artemisinin-resistant HRP2-negative malaria in Eritrea. *N. Engl. J. Med.* **389**, 1191–1202 (2023).

19. Fola, A. A. *et al.* Plasmodium falciparum resistant to artemisinin and diagnostics have emerged in Ethiopia. *Nat. Microbiol.* **8**, 1911–1919 (2023).

20. Ishengoma, D. S. *et al.* Evidence of artemisinin partial resistance in northwestern Tanzania: clinical and molecular markers of resistance. *Lancet Infect. Dis.* **24**, 1225–1233 (2024).

21. Tumwebaze, P. K. *et al.* Decreased susceptibility of Plasmodium falciparum to both dihydroartemisinin and lumefantrine in northern Uganda. *Nat. Commun.* **13**, 6353

(2022).

22. Okitwi, M. *et al.* Changes in susceptibility of Plasmodium falciparum to antimalarial drugs in Uganda over time: 2019-2024. *medRxiv* (2025) doi:10.1101/2024.12.31.24319821.

23. Venkatesan, M. *et al.* Polymorphisms in Plasmodium falciparum chloroquine resistance transporter and multidrug resistance 1 genes: parasite risk factors that affect treatment outcomes for P. falciparum malaria after artemether-lumefantrine and artesunate-amodiaquine. *Am. J. Trop. Med. Hyg.* **91**, 833–843 (2014).

24. Fançony, C. *et al.* Artemether-Lumefantrine treatment selects Plasmodium falciparum multidrug resistance 1 (pfmdr1) increased copy number among African malaria infections. *J. Infect. Dis.* (2025) doi:10.1093/infdis/jiaf155.

25. Tumwebaze, P. K. *et al.* Drug susceptibility of Plasmodium falciparum in eastern Uganda: a longitudinal phenotypic and genotypic study. *Lancet Microbe* **2**, e441–e449 (2021).

26. Mungthin, M. *et al.* Association between the pfmdr1 gene and in vitro artemether and lumefantrine sensitivity in Thai isolates of Plasmodium falciparum. *Am. J. Trop. Med. Hyg.* **83**, 1005–1009 (2010).

27. Kubota, R., Ishino, T., Iwanaga, S. & Shinzawa, N. Evaluation of the effect of gene duplication by genome editing on drug resistance in Plasmodium falciparum. *Front. Cell. Infect. Microbiol.* **12**, 915656 (2022).

28. Laird, V. R. *et al.* Plasmodium falciparum multidrug resistance 1 gene polymorphisms associated with outcomes after anti-malarial treatment. *Malar. J.* **24**, 186 (2025).

29. Rasmussen, S. A. *et al.* Changing antimalarial drug sensitivities in Uganda. *Antimicrob. Agents Chemother.* **61**, (2017).

30. Ebong, C. *et al.* Efficacy and safety of artemether-lumefantrine and dihydroartemisinin-piperaquine for the treatment of uncomplicated Plasmodium falciparum malaria and prevalence of molecular markers associated with artemisinin and partner drug resistance in Uganda. *Malar. J.* **20**, 484 (2021).

31. Kamya, M. R. *et al.* Efficacies of artemether-lumefantrine, artesunate-amodiaquine, dihydroartemisininpiperaquine and artesunate-pyronaridine for the treatment of uncomplicated Plasmodium falciparum malaria in children in Uganda: A randomized, open-label phase IV clinical trial. *Social Science Research Network* (2025) doi:10.2139/ssrn.5226564.

32. Awor, P. *et al.* Indigenous emergence and spread of kelch13 C469Y artemisinin-resistant Plasmodium falciparum in Uganda. *Antimicrob. Agents Chemother.* **68**, e0165923 (2024).

33. Asua, V. *et al.* Changing prevalence of potential mediators of aminoquinoline, antifolate, and artemisinin resistance across Uganda. *J. Infect. Dis.* **223**, 985–994 (2021).

34. Niaré, K., Greenhouse, B. & Bailey, J. A. An optimized GATK4 pipeline for Plasmodium falciparum whole genome sequencing variant calling and analysis. *Malar. J.* **22**, 207 (2023).

35. Amambua-Ngwa, A. *et al.* Chloroquine resistance evolution in Plasmodium falciparum is mediated by the putative amino acid transporter AAT1. *Nat Microbiol* **8**, 1213–1226 (2023).

663 36. Mukherjee, A. *et al.* A Phosphoinositide-Binding Protein Acts in the Trafficking
664 Pathway of Hemoglobin in the Malaria Parasite Plasmodium falciparum. *MBio* **13**,
665 e0323921 (2022).
666 37. Zhu, L. *et al.* The origins of malaria artemisinin resistance defined by a genetic and
667 transcriptomic background. *Nat. Commun.* **9**, 5158 (2018).
668 38. Ravenhall, M. *et al.* Characterizing the impact of sustained
669 sulfadoxine/pyrimethamine use upon the Plasmodium falciparum population in
670 Malawi. *Malar. J.* **15**, 575 (2016).
671 39. Ocholla, H. *et al.* Whole-genome scans provide evidence of adaptive evolution in
672 Malawian Plasmodium falciparum isolates. *J. Infect. Dis.* **210**, 1991–2000 (2014).
673 40. Tang, W. K. *et al.* Multistage protective anti-CelTOS monoclonal antibodies with
674 cross-species sterile protection against malaria. *Nat. Commun.* **15**, 7487 (2024).
675 41. Lefebvre, M. J. M. *et al.* Population genomic evidence of adaptive response during
676 the invasion history of Plasmodium falciparum in the Americas. *Mol. Biol. Evol.*
677 (2023) doi:10.1093/molbev/msad082.
678 42. Shah, Z. *et al.* Whole-genome analysis of Malawian Plasmodium falciparum
679 isolates identifies possible targets of allele-specific immunity to clinical malaria.
680 *PLoS Genet.* **17**, e1009576 (2021).
681 43. Mobegi, V. A. *et al.* Genome-wide analysis of selection on the malaria parasite
682 Plasmodium falciparum in West African populations of differing infection endemicity.
683 *Mol. Biol. Evol.* **31**, 1490–1499 (2014).
684 44. MalariaGEN *et al.* An open dataset of Plasmodium falciparum genome variation in
685 7,000 worldwide samples. *Wellcome Open Res* **6**, 42 (2021).

686 45. van Schalkwyk, D. A. *et al.* Treatment failure in a UK malaria patient harboring
687 genetically variant Plasmodium falciparum from Uganda with reduced in vitro
688 susceptibility to artemisinin and lumefantrine. *Clin. Infect. Dis.* **78**, 445–452 (2024).
689 46. Sutherland, C. J. *et al.* Pfk13-independent treatment failure in four imported cases
690 of Plasmodium falciparum malaria treated with artemether-lumefantrine in the
691 United Kingdom. *Antimicrob. Agents Chemother.* **61**, (2017).
692 47. Oliveira, R. *et al.* Artemether-lumefantrine resistant falciparum malaria imported
693 from Uganda. *J. Travel Med.* (2025) doi:10.1093/jtm/taaf013.
694 48. Henden, L., Lee, S., Mueller, I., Barry, A. & Melanie Bahlo. Identity-by-descent
695 analyses for measuring population dynamics and selection in recombining
696 pathogens. *PLoS Genet.* **14**, e1007279 (2018).
697 49. Asua, V. *et al.* Changing molecular markers of antimalarial drug sensitivity across
698 Uganda. *Antimicrob. Agents Chemother.* **63**, (2019).
699 50. Yeka, A. *et al.* Artemisinin versus nonartemisinin combination therapy for
700 uncomplicated malaria: randomized clinical trials from four sites in Uganda. *PLoS*
701 *Med.* **2**, e190 (2005).
702 51. Oyola, S. O. *et al.* Whole genome sequencing of Plasmodium falciparum from dried
703 blood spots using selective whole genome amplification. *Malar. J.* **15**, 597 (2016).
704 52. Miles, A. *et al.* Indels, structural variation, and recombination drive genomic
705 diversity in Plasmodium falciparum. *Genome Res.* **26**, 1288–1299 (2016).
706 53. Chang, H.-H. *et al.* THE REAL McCOIL: A method for the concurrent estimation of
707 the complexity of infection and SNP allele frequency for malaria parasites. *PLoS*
708 *Comput. Biol.* **13**, e1005348 (2017).

54. Gautier, M. & Vitalis, R. rehh: an R package to detect footprints of selection in genome-wide SNP data from haplotype structure. *Bioinformatics* **28**, 1176–1177 (2012).

55. Meier-Scherling, C. P. G. *et al.* Selection of artemisinin partial resistance Kelch13 mutations in Uganda in 2016-22 was at a rate comparable to that seen previously in South-East Asia. *medRxiv* (2024) doi:10.1101/2024.02.03.24302209.

Extend Data Figures

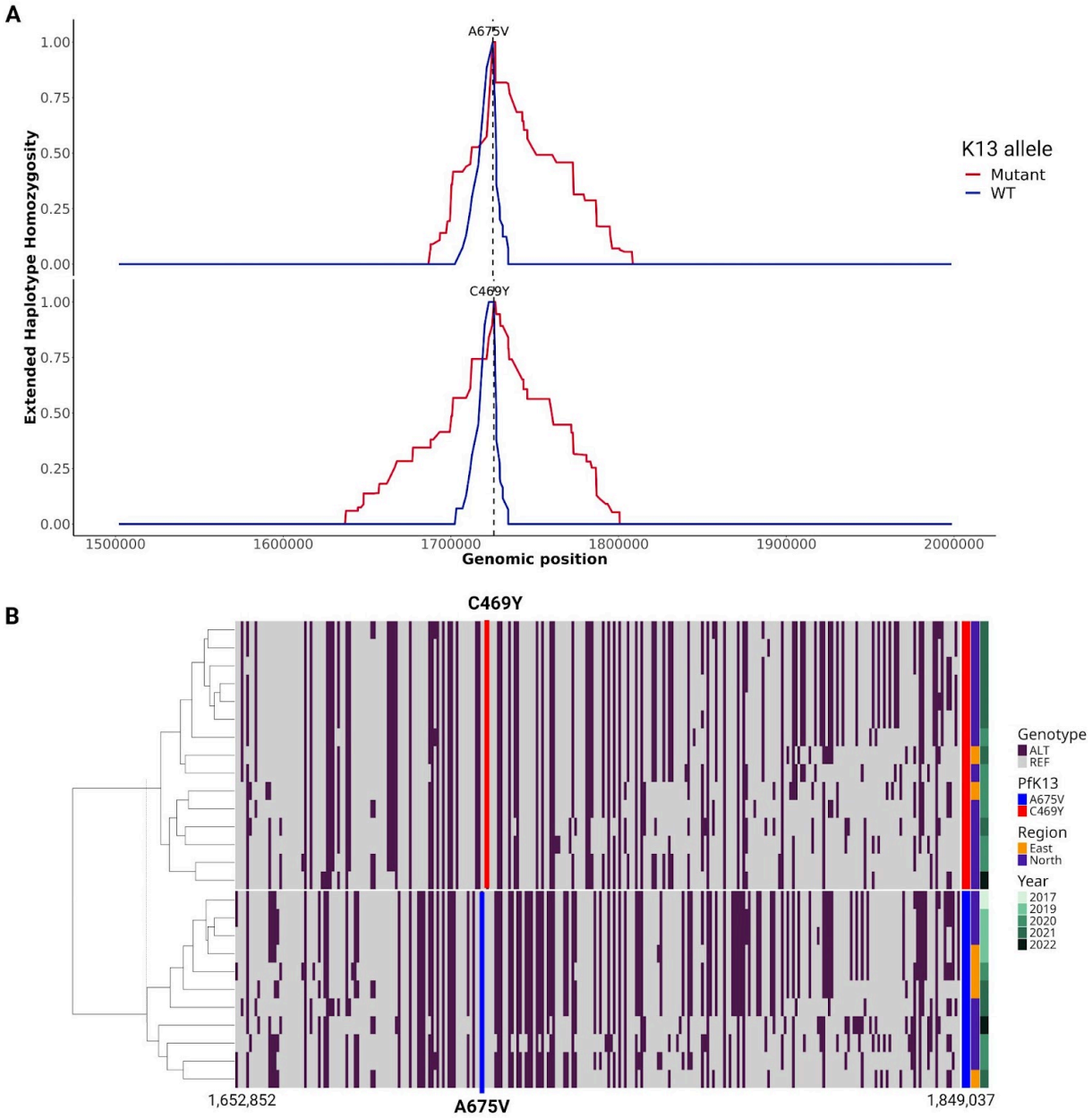

Extended Data Figure 1: Signal of selection around K13 mutations C469Y and A675V. **A)** Decay of the extended haplotype homozygosity around each of the two markers (n=158). Mutant (red) represents 469Y or 675V. Analysis included dominant alleles with minor allele frequency ≥2%. **B)** Visualization and hierarchical clustering of flanking haplotypes based on genotypes. Region size was based on the maximal extended haplotype heterozygosity region found in **(A)** and measured ~200kb. Positions of key mutations are highlighted by red and blue vertical lines.

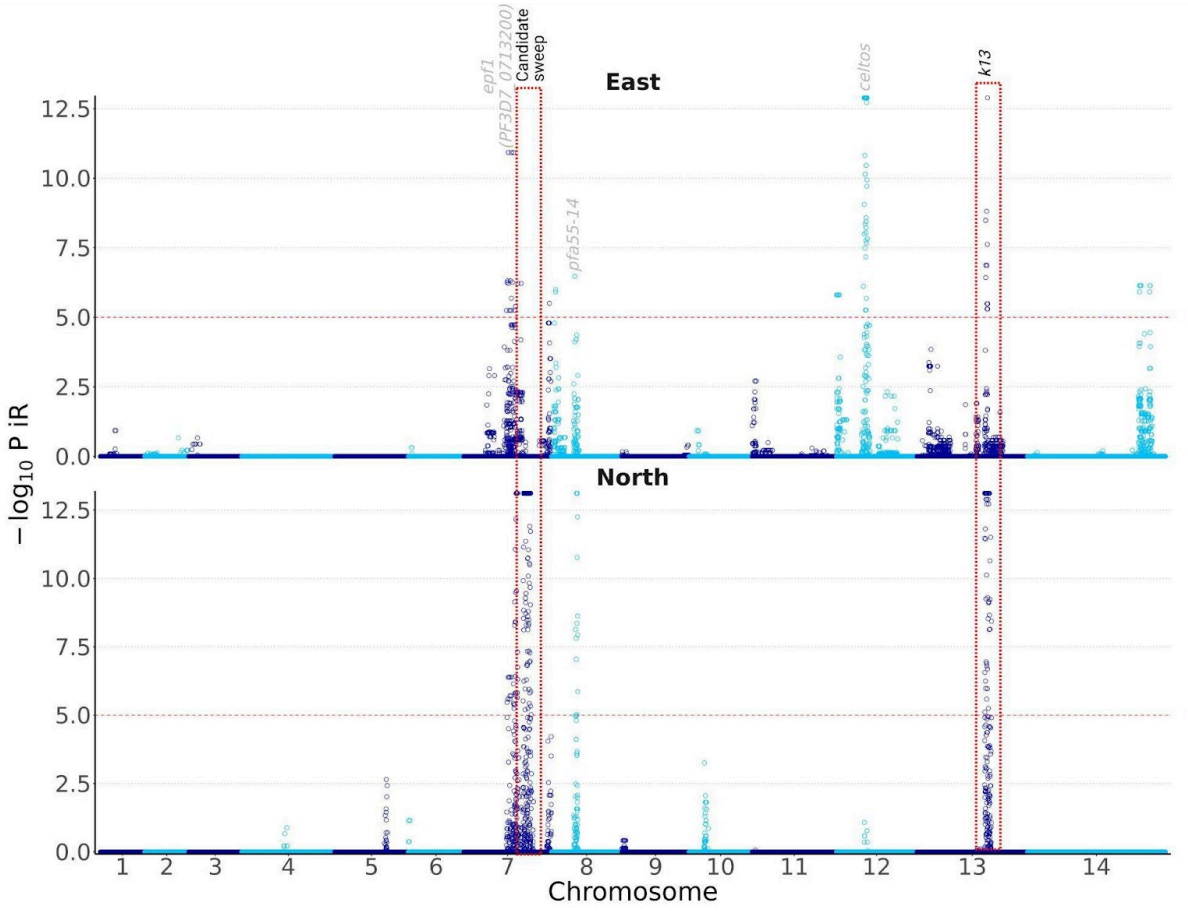

Extended Data Figure 2: Selection signals by region. *P* values were corrected for multiple testing using false discovery rate. Significance threshold of -Log_{10}(FDR-corrected *P* value) of 5 was indicated by the red dotted horizontal line. Red dashed rectangles demarcate candidate sweep and *k13* peak. The analysis included SNPs with minor allele frequency ≥2% and all samples (n=158). Genes corresponding to peaks are indicated.

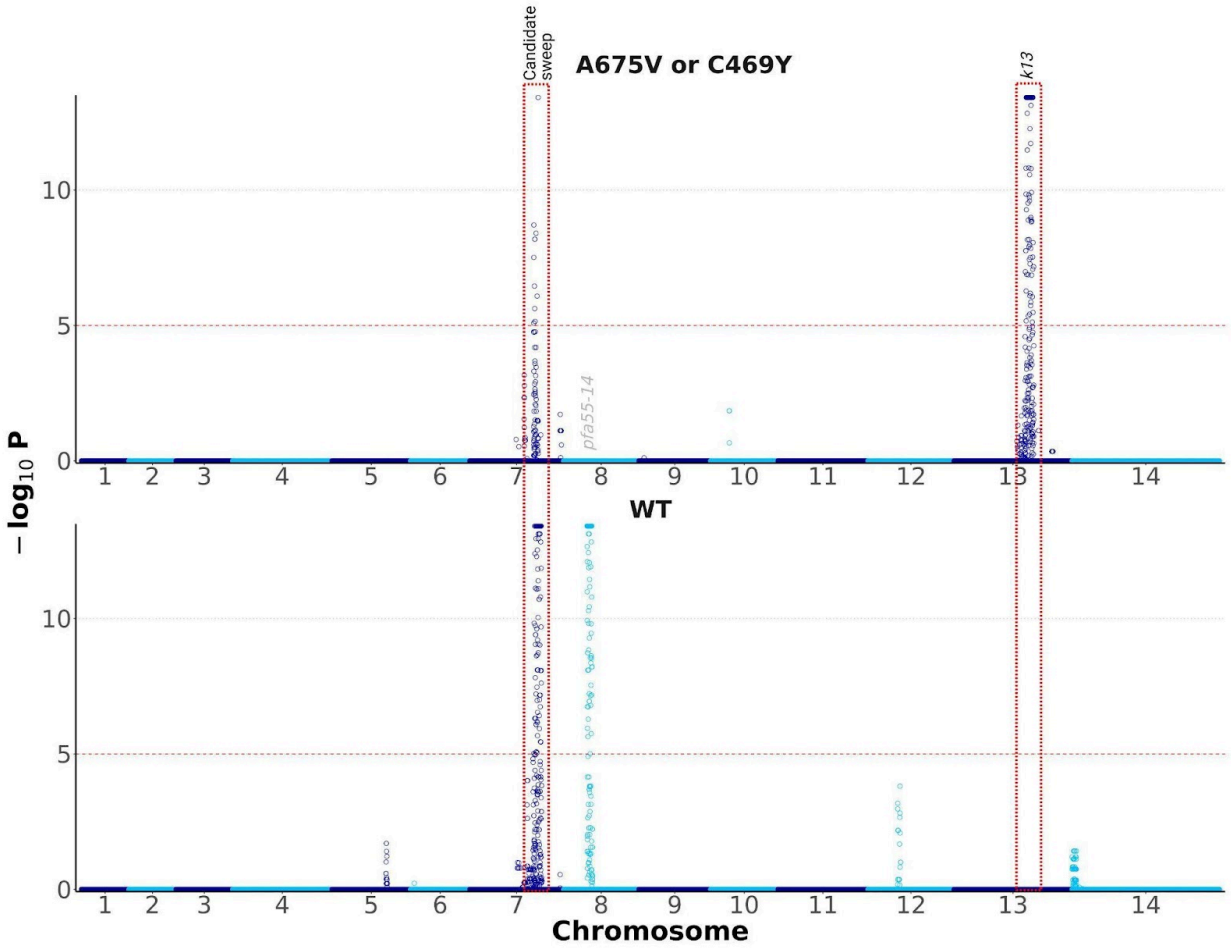

Extended Data Figure 3: Selection signal by K13 genotype. *P* values were corrected for multiple testing using false discovery rate. Significance threshold of -Log_{10}(FDR-corrected *P* value) of 5 was indicated by the red dotted horizontal line. The analysis included SNPs with minor allele frequency ≥2% and all samples (n=158). Genes corresponding to peaks are indicated. Red dashed rectangles demarcate candidate sweep and *k13* peak.

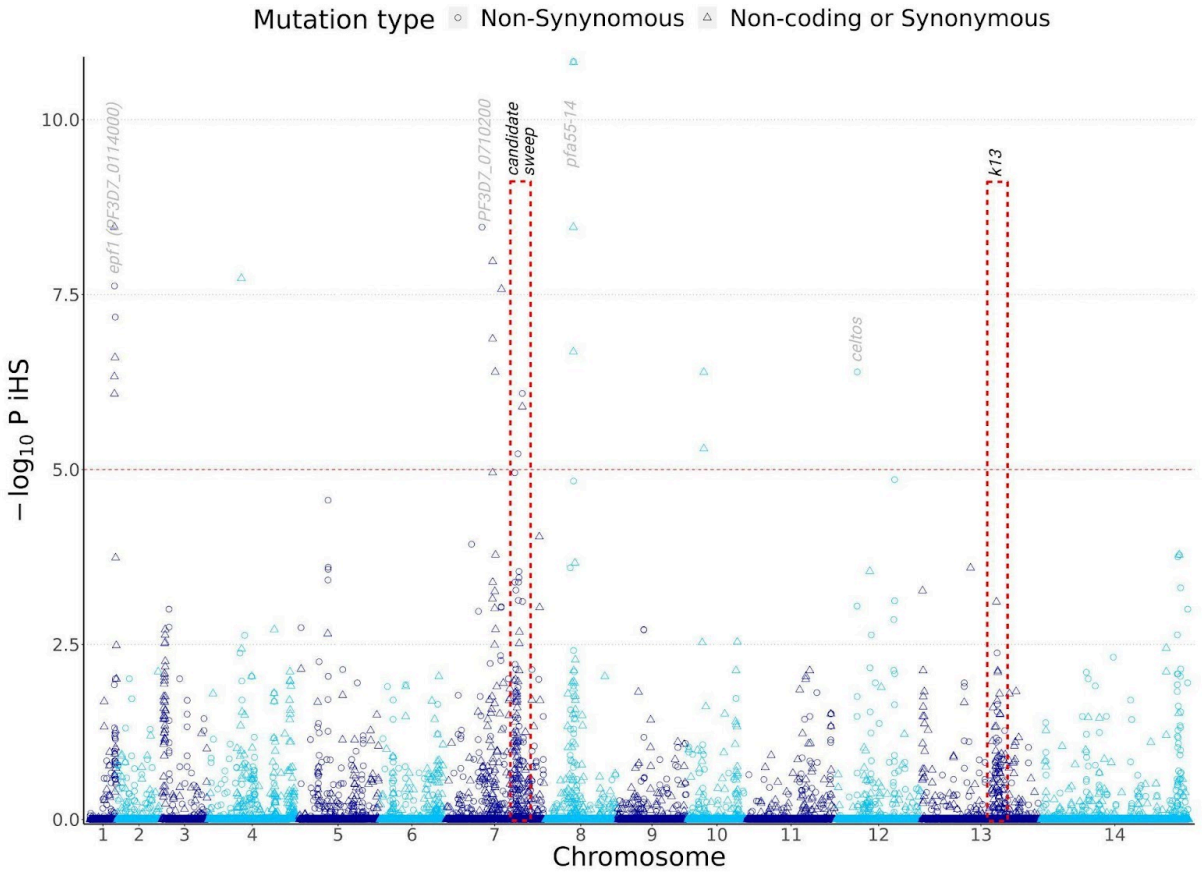

Extended Data Figure 4: Unfiltered iHS signals. *P* values were corrected for multiple testing using false discovery rate. Significance threshold of -Log10(FDR-corrected *P* value) of 5 was indicated by the red dotted horizontal line. Red dashed rectangles demarcate candidate sweep and *k13* peak. The analysis included SNPs with minor allele frequency ≥2% and mono-genomic samples (n=118). *epf1*: *exported protein 1*; *celtos: cell-traversal protein for ookinetes and sporozoites; pfa55-14: asparagine-rich antigen.*

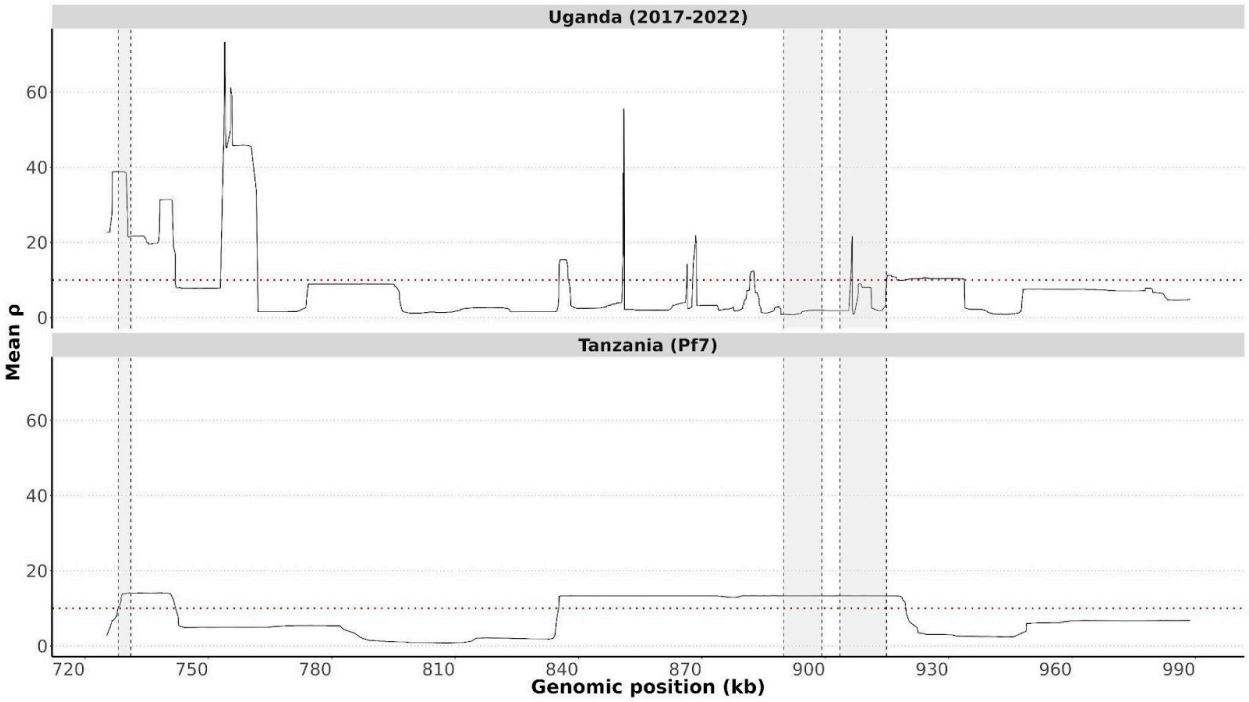

Extended Data Figure 5: Genetic recombination map of the candidate sweep region. This analysis included SNPs with minor allele frequency ≥2% and mono-genomic samples in our study (n=118) and MalariaGEN Pf7 (n=96). The *px1* gene had lowest ρ values, ranging between 0.78-1.97. PF3D7_0721000 had high ρ values, ranging between 0.99-21.60.

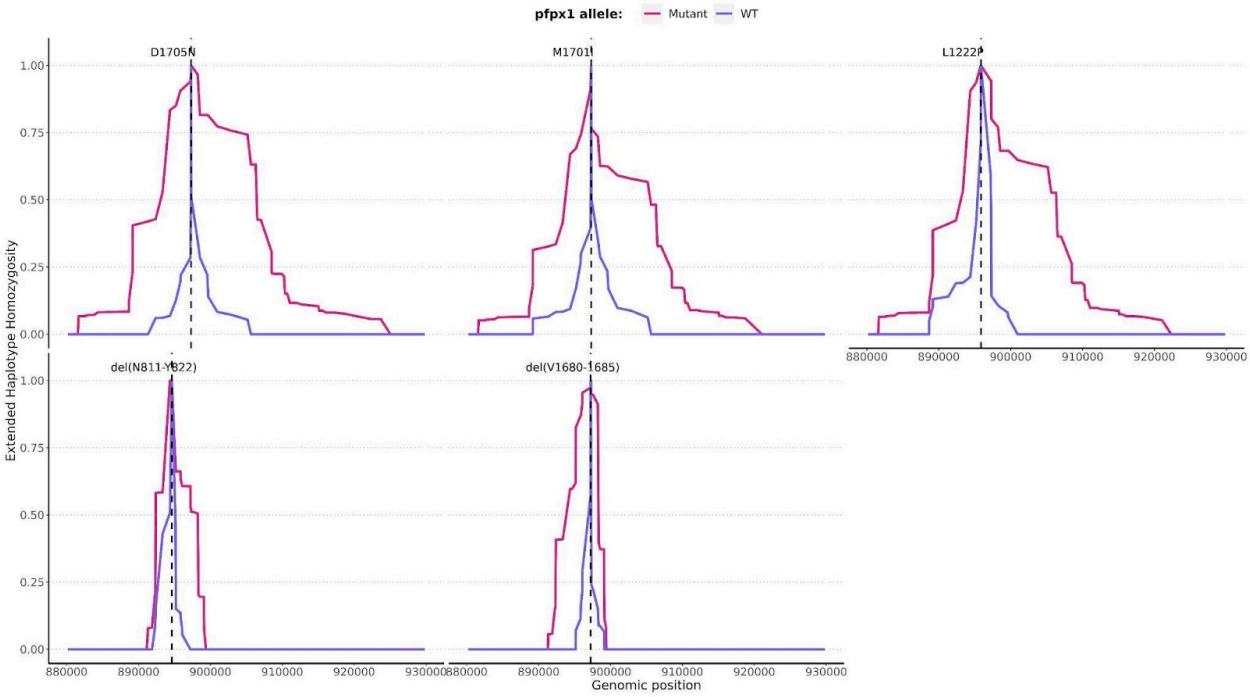

Extended Data Figure 5: Extended haplotype homozygosity profile for PX1 top variants (SNPs and indels). WT: wild-type. The analysis included SNPs and indels with minor allele frequency ≥2% and mono-genomic samples (n=118). The two deletions ($del_{V16Z80\text{-}1685}$ and $del_{N1289\text{-}1294}$) were rare in global populations and belonged in the PIN haplotype.